scientific reports

Check for updates

OPEN

Structural characterization, thermal properties, and molecular motions near the phase transition in hybrid perovskite $[(CH_2)_3(NH_3)_2]CuCl_4$ crystals: ^1H, ^{13}C, and ^{14}N nuclear magnetic resonance

Ae Ran Lim

The structural characterization of the $[(CH_2]_3(NH_3)_2]^+$ cation in the perovskite $[(CH_2)_3(NH_3)_2]CuCl_4$ crystal was performed by solid-state ^1H nuclear magnetic resonance (NMR) spectroscopy. The ^1H NMR chemical shifts for NH_3 changed more significantly with temperature than those for CH_2. This change in cationic motion is enhanced at the N-end of the organic cation, which is fixed to the inorganic layer by N–H···Cl hydrogen bonds. The ^{13}C chemical shifts for CH_2-1 increase slowly without any anomalous change, while those for CH_2-2 move abruptly compared to CH_2-1 with increasing temperature. The four peaks of two groups in the ^{14}N NMR spectra, indicating the presence of a ferroelastic multidomain, were reduced to two peaks of one group near T_{C2} (= 333 K); the ^{14}N NMR data clearly indicated changes in atomic configuration at this temperature. In addition, ^1H and ^{13}C spin–lattice have shorter relaxation times ($T_{1\rho}$), in the order of milliseconds because $T_{1\rho}$ is inversely proportional to the square of the magnetic moment of paramagnetic ions. The $T_{1\rho}$ values for CH_2 and NH_3 protons were almost independent of temperature, but the CH_2 moiety located in the middle of the N–C–C–C–N bond undergoes tumbling motion according to the Bloembergen–Purcell–Pound theory. Ferroelasticity is the main cause for the phase transition near T_{C2}.

The hybrid organic–inorganic compounds, $[(CH_2)_n(NH_3)_2]MX_4$ (M = Mn, Fe, Co, Cu, and Cd, X = Cl, Br, n = 2, 3 …), are well-known, and have been studied extensively for groups of these crystals. Most of these structures exhibit ferroelastic or ferroelectric phase transitions. The physical properties and phase transitions are related to their structure and the interaction between cationic and anionic sublattices. An interesting family of hybrid compounds is perovskite-type crystals with $(CH_2)_n(NH_3)_2$ and MX_4-layered metal-halogen anionic sublattice[1–8]. In $[(CH_2)_n(NH_3)_2]MX_4$, the hydrogen bonds form between the NH_3 groups at both ends of the aliphatic chains and X-atoms of the perovskite-type layer. Hybrid organic–inorganic materials based on the perovskite structures are interesting owing to their potential applications[9–15]. On the one hand, the ferroelastic orientation state in a material is determined by its spontaneous strain tensor, similar to how spontaneous polarization leads to ferroelctricity[16]. Moreover, ferroelasticity is commonly observed in materials with a perovskite crystal structure. Recently, the ferroelastic twin domain observed in hybrid organic–inorganic perovskite has also garnered much attention[17–19].

Among these materials, $[(CH_2)_3(NH_3)_2]CuCl_4$ [bis (propylene-1, 3-diammonium) tetrachlorocuprate] with n = 3 and M = Cu undergoes two phase transitions, at temperatures of 333 K (= T_{C2}) and 434 K (= T_{C1})[20].

The crystal at room temperature has an orthorhombic structure with a space group *Pnma*. The unit cell dimensions are a = 7.202 Å, b = 18.260 Å, c = 7.515 Å, and Z = 4[21]. The crystal structure consists of chloro-bridged deformed tetragonal $(CuCl_4)^{2-}$ to form two-dimensional layers. The chlorocuprate sheet is hydrogen bonded to $[(CH_2)_3(NH_3)_2]$ in alternating layers. The structural geometry of the $[(CH_2)_3(NH_3)_2]CuCl_4$ is shown in Fig. 1[21]. Extensive hydrogen bonding of the N–H···Cl occurs between the Cu–Cl layer and the alkylammonium chain.

Analytical Laboratory of Advanced Ferroelectric Crystals, Department of Science Eduction, Jeonju University, Jeonju 55069, Korea. email: arlim@jj.ac.kr

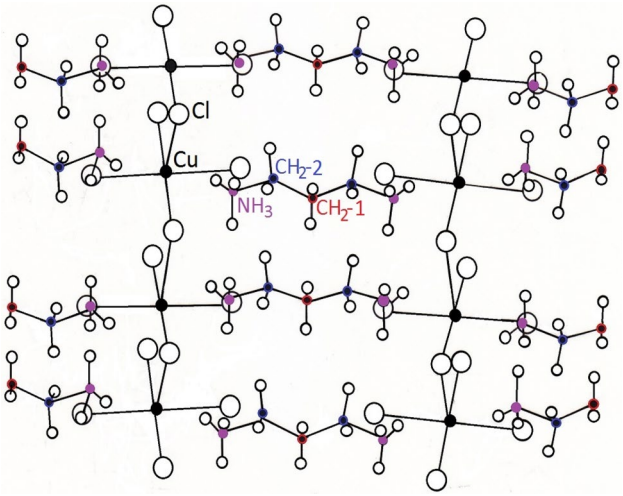

Figure 1. Structural geometry of $[(CH_2)_3(NH_3)_2]CuCl_4$ at room temperature. Here, CH_2 between CH_2 and CH_2 is named CH_2-1, and CH_2 close to NH_3 is named CH_2-2.

The organic chains are extended along the *a* direction. The organic chains NH_3–CH_2–CH_2–CH_2–NH_3 are almost identical, and the skeleton N–C–C–C–N is planar. Above 434 K, the symmetry is monoclinic with space group *B2/m* and lattice constants $a = 7.309$ Å, $b = 8.866$ Å, $c = 7.614$ Å, $\alpha = 95.365°$, and $Z = 2$[22]. The lattice constants *a* and *c* in the monoclinic structure are comparable with those in the room temperature structure, whereas the *b* parameter in the monoclinic structure is half of that in the room temperature structure.

According to the previously reported, the Phelps et al.[21] and Czupinski et al.[23] determined the structural phase transition for $(CH_2)_3(NH_3)_2CuCl_4$. And, the structural, dielectric, and conductive properties were discussed by Mostafa et al.[20]. In addition, the structural phase transition was analysed by x-ray and optical studies[22], where ferroelastic multidomain walls were observed in the orthorhombic phase. Iqbal et al.[1] reported Raman scattering results at various temperatures above and below the respective magnetic ordering temperature (149 K) and in a magnetic field up to 10 kg. The crystal structure, magnetic and optical properties have been studied by only a few researchers. In addition, the thermal properties, the structural and molecular dynamics of the $[(CH_2)_3(NH_3)_2]CuCl_4$ crystal have not been studied in detail.

Here, differential scanning calorimetry (DSC) and thermogravimetric analysis (TGA) experiments were performed to provide a better understanding of the phase transition temperatures and thermal properties of $[(CH_2)_3(NH_3)_2]CuCl_4$. In addition, the structural characterizations of the $[(CH_2)_3(NH_3)_2]$ cation were studied in detail by magic angle spinning (MAS) nuclear magnetic resonance (NMR) and static NMR methods. The temperature dependences of the chemical shifts and spin–lattice relaxation times $T_{1\rho}$ were measured by ^{1}H MAS NMR and ^{13}C cross-polarization (CP)/MAS NMR to highlight the role of the cation in $[(CH_2)_3(NH_3)_2]CuCl_4$. In addition, ^{14}N static NMR spectra of $[(CH_2)_3(NH_3)_2]CuCl_4$ single crystals were acquired. Based on these results, the structural characterizations for NH_3–CH_2–CH_2–CH_2–NH_3 are discussed as a function of temperature. In particular, the hydrogen bonding of the N–H···Cl between the Cu–Cl layer and the alkylammonium chain within the $[(CH_2)_3(NH_3)_2]CuCl_4$ is expected to give important information regarding the fundamental mechanisms that enable various potential applications.

Experimental

Crystals of $[(CH_2)_3(NH_3)_2]CuCl_4$ were prepared by mixing equimolar amounts of $NH_2(CH_2)_3NH_2{\cdot}2HCl$ and $CuCl_2$ (1:1 ratio) in aqueous solution. Then, the resulting mixture was allowed to slowly evaporate at 300 K. The crystals grew as rectangular parallelepipeds, with dimensions of $7 \times 7 \times 2$ mm^3.

The structure of the $[(CH_2)_3(NH_3)_2]CuCl_4$ crystal at 300 K was analysed using an X-ray diffraction system equipped with a Cu-Kα radiation source at the KBSI, Seoul Western Center. DSC (TA Instruments, DSC 25) was conducted at a heating rate of 10 °C/min from 190 to 600 K under nitrogen gas. TGA was performed using a thermogravimetric analyser (TA Instruments) from 300 to 680 K at the same heating rate. The sample weights used for DSC and TGA experiments were 6.23 and 7.53 mg, respectively. Optical observations were performed using an optical polarized microscope in the temperature range of 300–600 K, where the as-grown crystals were placed on a Linkam THM-600 heating stage.

NMR spectra of $[(CH_2)_3(NH_3)_2]CuCl_4$ crystals were obtained using a 400 MHz Avance II + Bruker solid-state NMR spectrometer, equipped with 4 mm CP/MAS probes (at the KBSI, Seoul Western Center). The Larmor frequencies to ^{1}H MAS NMR and ^{13}C CP/MAS NMR experiments were at $\omega_0/2\pi = 400.13$ and 100.61 MHz, respectively. A MAS rate of 10 kHz was used to minimize the spinning sideband. The NMR chemical shifts were recorded using tetramethylsilane (TMS) as the standard. The $T_{1\rho}$ values were measured using a $\pi/2 - t$ sequence by changing the spin-locking pulses, and the width of the $\pi/2$ pulse was 3.3 μs. The spin-lock power on the ^{1}H and ^{13}C channel was 75.76 kHz. The ^{13}C $T_{1\rho}$ values were obtained by changing the duration of the ^{13}C spin-locking

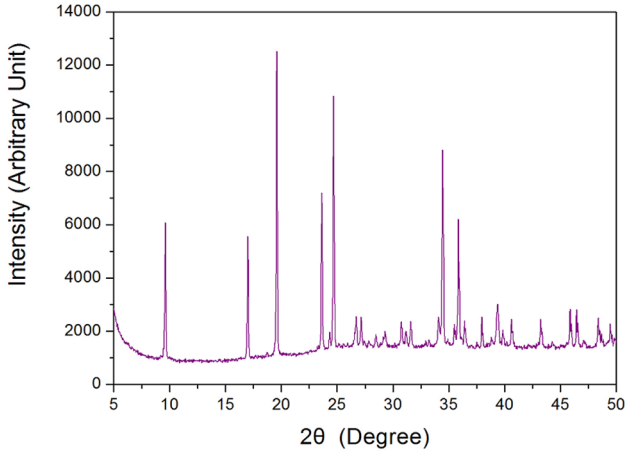

Figure 2. X-ray diffraction pattern of the $[(CH_2)_3(NH_3)_2]CuCl_4$ crystal at 300 K.

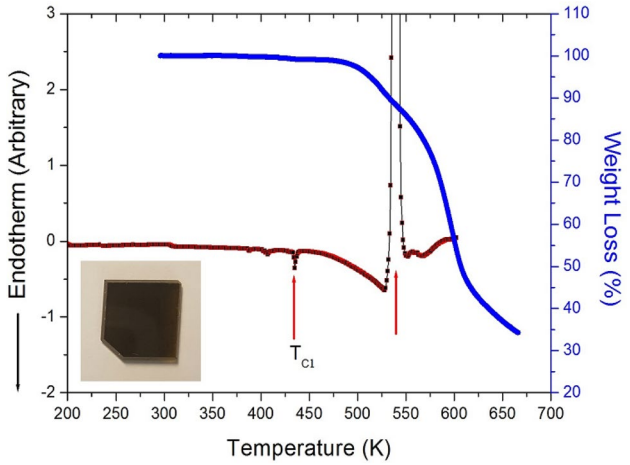

Figure 3. Thermogravimetric analysis (TGA) and differential scanning calorimetry (DSC) thermogram of $[(CH_2)_3(NH_3)_2]CuCl_4$ (Inset: photograph of the crystal at 300 K).

pulse applied after the CP preparation period. In addition, ^{14}N NMR spectra of a $[(CH_2)_3(NH_3)_2]CuCl_4$ single crystal were measured with a Larmor frequency of 28.90 MHz. The resonance frequency was referenced with respect to NH_3NO_3 as a standard sample. The ^{14}N NMR experiments were performed using a solid-state echo sequence: 8 μs—tau (16 μs) – 8 μs—tau (16 μs). NMR data could not be obtained because the NMR spectrometer could not operate at temperatures above 430 K. The true temperature at spinning condition of 10 kHz was adjusted based on the sample temperature, suggested by Guan and Stark[24]. The temperature change was maintained within the error range of ± 0.5 K while adjusting nitrogen gas flow and heater current.

Experimental results

The X-ray powder diffraction pattern of the $[(CH_2)_3(NH_3)_2]CuCl_4$ crystal at room temperature is displayed in Fig. 2, and this result was consistent with that reported by Czapla et al.[23] The results of the DSC analysis of $[(CH_2)_3(NH_3)_2]CuCl_4$ under a nitrogen atmosphere are shown in Fig. 3. An endothermic peak at 434 K and a exothermic peak at 539 K where observed. However, the peak around 334 K reported previously[20] was not observed. To confirm that the DSC peaks at 434 K and 539 K were consistent with the structural phase transition, TGA was performed. The measured TGA curves are also shown in Fig. 3. Good thermal stability was observed up to around 480 K; above this temperature, the first signs of weight loss were observed, indicating the onset of partial thermal decomposition. The crystalline structure of the compound $[(CH_2)_3(NH_3)_2]CuCl_4$ (M = 280.49 mg) breaks down at high temperatures. Considering the TGA results and possible chemical reactions, the solid residue amounts were calculated. The weight loss of 13% at around 539 K (see Fig. 3) was likely due to the decomposition of the HCl moieties, which is consistent with the exothermic peak at the same temperature in the DSC curve. The weight sharply decreased between 500 and 600 K, with a corresponding weight loss of 65% around 650 K. This result is consistent with previous TGA data[23]. Further, optical polarizing microscopy was used to understand the crystal's phase transition, thermal decomposition, and melting mechanism. The color of the crystal was dark

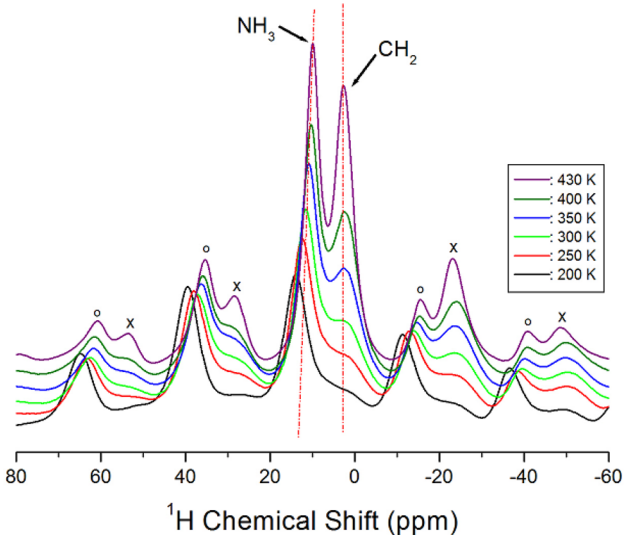

Figure 4. ^{1}H MAS NMR spectra for CH_2 and NH_3 of $[(CH_2)_3(NH_3)_2]CuCl_4$ at various temperatures (spinning sidebands are indicated by cross and open circles).

brown at room temperature, as illustrated in the inset of Fig. 3. While there were no changes observed from room temperature to 523 K, it began to melt slightly at approximately 539 K. Above 600 K, the crystal emitted an odour, and its surface and edges melted considerably (see Suppplementary Information 1).

The chemical shifts of the ^{1}H NMR spectrum of $[(CH_2)_3(NH_3)_2]CuCl_4$ crystals were obtained with increasing temperature, as shown in Fig. 4. Two peaks in the NMR spectra are indicated in the figure; the spinning sidebands for CH_2 are represented with crosses, and those for NH_3 are marked with open circles. At 300 K, the ^{1}H NMR chemical shift for CH_2 was observed at $\delta = 2.76$ ppm, whereas that for NH_3 was at $\delta = 11.48$ ppm. Below 300 K, the signal for ^{1}H of CH_2 had very low intensity and could not be easily identified. The ^{1}H peak for CH_2 did not significantly change with increasing temperature, while for NH_3, the change in the chemical shift was dependent on temperature (see the Supplementary Information 2).

The ^{1}H NMR spectra were also measured with several delay times, and the intensity of NMR spectra as a function of delay time followed a single exponential function. The rate of decay of the spin-locked proton magnetization is characterized by $T_{1\rho}$[25–27]:

$$I(t) = I(0)\exp(-t/T_{1\rho}), \quad (1)$$

where $I(t)$ and $I(0)$ are the signal intensity at time t and $t = 0$, respectively. The ^{1}H NMR signals of CH_2 and NH_3 measured at 300 K were plotted as a function of delay time over the range of 0.2–80 ms, as shown in the inset of Fig. 5. It can be seen that the ^{1}H NMR signal intensities varied with the delay time. From the slope of the intensity vs. delay time curve, ^{1}H $T_{1\rho}$ values for $[(CH_2)_3(NH_3)_2]CuCl_4$ were obtained from the CH_2 and NH_3 peaks as a function of inverse temperature. Changes in $T_{1\rho}$ values above T_{C1} were not observed outside this temperature because of the limitation of the NMR spectrometer. The ^{1}H $T_{1\rho}$ values for CH_2 and NH_3 were of the order of 10 ms, and their values were almost independent of temperature (see Fig. 5).

The ^{13}C NMR chemical shifts for CH_2 in $[(CH_2)_3(NH_3)_2]CuCl_4$ were measured as a function of temperature, as shown in Fig. 6. At all temperatures, the ^{13}C MAS NMR spectra showed two resonance signals. The ^{13}C MAS NMR spectrum for TMS was observed at 38.3 ppm at 300 K, which was used to calibrate the device to 0 ppm for determining the chemical shift in ^{13}C[28]. Here, CH_2 between CH_2 and CH_2 is named CH_2-1, and CH_2 close to NH_3 is named CH_2-2. At 300 K, the two resonance signals were recorded at chemical shifts of $\delta = 28.78$ and $\delta = 124.97$ ppm for CH_2-1 and CH_2-2, respectively. The ^{13}C chemical shifts for CH_2 were different CH_2-1 far away from NH_3 and CH_2-2 close to NH_3. The small ^{13}C resonance peaks indicated by arrow at 420 K and 430 K were attributed to a splitting of the CH_2-2. The ^{13}C chemical shift for CH_2-1 increased slowly and monotonously without an anomalous change with increasing temperature, whereas those for CH_2-2 moved abruptly to the lower side with increasing temperature compared to CH_2-1, as shown in the inset in Fig. 6.

The ^{13}C full-width at half-maximum (FWHM) values of the NMR peaks for CH_2-1 and CH_2-2 decreased with increasing temperature. Broader line widths are observed for more rigid lattices, where motional narrowing is quenched, as shown by the increase in line widths at lower temperatures. The line widths of ^{13}C for CH_2-1 and CH_2-2 were the same within experimental uncertainty, where the line width narrowed from 30 to 10 ppm with increasing temperature from 180 to 430 K, respectively (see the Supplementary Information 3).

The integration change of the ^{13}C NMR spectra obtained by increasing the delay time was measured. All decay curves for CH_2-1 and CH_2-2 were described by a single exponential function, as shown by Eq. (1). ^{13}C $T_{1\rho}$ values were measured by the spin-locking pulse sequence with a locking pulse of 75.76 kHz. From the slope of their recovery traces, the ^{13}C $T_{1\rho}$ values were obtained for the CH_2-1 and CH_2-2 as a function of 1000/temperature, as shown in Fig. 7. Although no change in $T_{1\rho}$ values was observed near T_{C2}, $T_{1\rho}$ values measured for 180–430 K

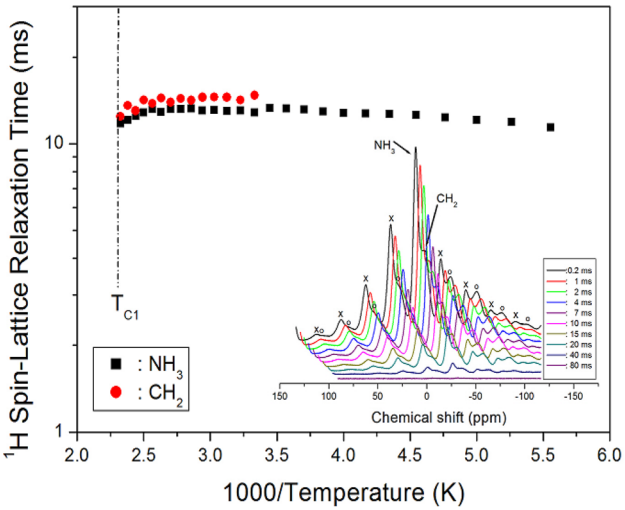

Figure 5. ^{1}H NMR spin–lattice relaxation times $T_{1\rho}$ for CH_2 and NH_3 ions of $[(CH_2)_3(NH_3)_2]CuCl_4$ as a function of inverse temperature (inset: ^{1}H NMR spectrum at several delay times at 300 K).

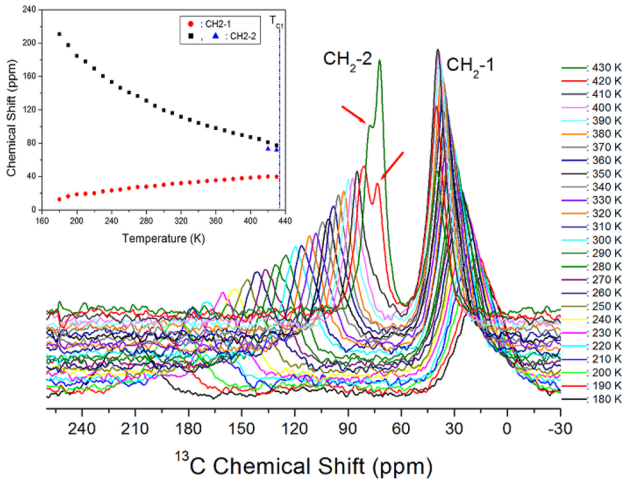

Figure 6. ^{13}C chemical shifts for CH_2-1 and CH_2-2 of $(CH_2)_3(NH_3)_2CuCl_4$ as a function of temperature.

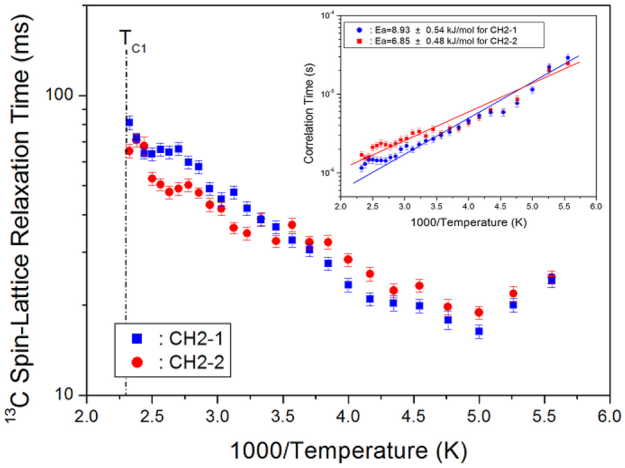

Figure 7. ^{13}C NMR spin–lattice relaxation times $T_{1\rho}$ for CH_2-1 and CH_2-2 of $[(CH_2)_3(NH_3)_2]CuCl_4$ as a function of inverse temperature (Inset: Correlation times for CH_2-1 and CH_2-2 in $[(CH_2)_3(NH_3)_2]CuCl_4$ as a function of inverse temperature. Solid lines represent the activation energies).

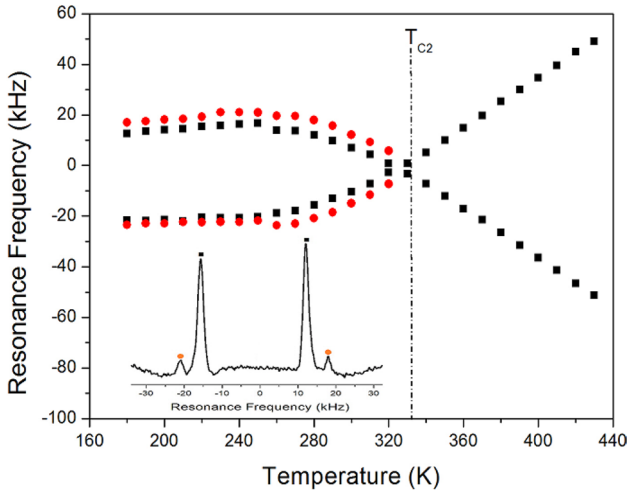

Figure 8. Temperature dependences on ^{14}N resonance frequency of $[(CH_2)_3(NH_3)_2]$ $CuCl_4$ single crystal (Inset: static ^{14}N NMR spectrum at 300 K).

indicated a much slower dynamics of carbon motion. The $T_{1\rho}$ vs. temperature curve showed minima of 16.32 and 18.87 ms for CH_2-1 and CH_2-2 at 200 K, respectively. This trend indicates that distinct molecular motions exist, where the minimum $T_{1\rho}$ was attributed to the uniaxial rotation of CH_2 ions. The $T_{1\rho}$ values were described by the correlation time τ_C for molecular motion, based on the theory of Bloembergen–Purcell–Pound (BPP). The $T_{1\rho}$ value for the molecular motion is given by[27,29]:

$$T_{1\rho}^{-1} = C\left(\gamma_I^2\gamma_e^2\mu_B^2 S(S+1)/r^6\right)\left[4f_a + f_b + 3f_c + 6f_d + 6f_e\right] \quad (2)$$

where $f_a = \tau_C/[1+\omega_1{}^2\tau_C{}^2]$, $f_b = \tau_C/[1+(\omega_C-\omega_e)^2\tau_C{}^2]$, $f_c = \tau_C/[1+\omega_C{}^2\tau_C{}^2]$, $f_d = \tau_C/[1+(\omega_C+\omega_e)^2\tau_C{}^2]$, and $f_e = \tau_C/[1+\omega_e{}^2\tau_C{}^2]$. Here, C is a coefficient, γ_e is the gyromagnetic ratio of the electron, S is the spin number of the paramagnetic ion, r is the distance between the paramagnetic ion and the carbon, ω_e is the Larmor frequency of electron, and ω_1 is the spin-lock field. When $\omega_C\tau_C = 1$, $T_{1\rho}$ is at its minimum, so a relationship between $T_{1\rho}$ and ω_1 was applied to obtain the coefficient in Eq. (2). Using this coefficient, we calculated τ_C as a function of temperature. According to BPP theory, the local field fluctuation is governed by the thermal motion of CH_2-1 and CH_2-2, which is activated by thermal energy. In this case, τ_C is described by Arrhenius behaviour: $\tau_C = \tau_o\exp(-E_a/k_BT)$, where τ_o, E_a, and k_B are the pre-correlation time, activation energy of the motions, and Boltzmann constant, respectively[27]. As the magnitude of E_a depends on the molecular dynamics, we plotted τ_C vs. 1000/T on a logarithmic scale (inset of Fig. 7), which gave E_a values for CH_2-1 and CH_2-2 of 8.93 ± 0.54 and 6.85 ± 0.48 kJ/mol, respectively.

^{14}N NMR investigations were performed using a $[(CH_2)_3(NH_3)_2]CuCl_4$ single crystal over the temperature range of 180–430 K. The ^{14}N spectra were obtained using the solid-state echo method by static NMR at a Larmor frequency of 28.90 MHz. Two ^{14}N NMR signals were derived from the quadrupole interactions due to the spin number I = 1. Near 333 K (= T_{C2}), the number of resonance lines and resonance frequency of the NMR spectrum showed abruptly changes, as shown in Fig. 8. Above T_{C2}, the spectrum showed one pair of lines, whereas below T_{C2} it showed two pairs. The lines with the same colour below T_{C2} indicate the same pairs for ^{14}N. The changes in the ^{14}N resonance frequency as a function of temperature were attributed to variations in the structural geometry, corresponding to changes in the quadrupole coupling constant[30,31]. The resonance frequency of the ^{14}N signals below T_{C2} changed almost continuously, and those of the ^{14}N signal above this temperature also varied abruptly. Near T_{C2}, the electric field gradient tensors at N sites varied, reflecting changes in the atomic configuration around the nitrogen atom. Although the phase transition temperature at T_{C2} reported previously[20] was not observed in our DSC experimental results, the ^{14}N NMR spectrum showed changes near T_{C2}. The phase transition at T_{C2} exists, and ^{14}N in the NH_3 groups plays an import role in this phase transition. In contrast, the two different ^{14}N spectra below T_{C2} are thought to have two inequivalent N sites or be due to twin domains. However, according to the previouslyreported X-ray results[21], there have been no reports of two different N sites, and twin domains have been reported[22]. Czapla et al.[22] suggested that the ferroelastic domains observed in the orthorhombic phase could be connected to a prototype tetragonal phase. Here, the $[(CH_2)_3(NH_3)_2]CuCl_4$ crystal existed in three crystallographic phases: monoclinic (*2/m*) above 434 K, tetragonal (*4/mmm*) between 334 and 434 K, and orthorhombic (*mmm*) below 334 K. For the transition from the *4/mmm* of the tetragonal phase to the *mmm* of the orthorhombic phase, the domain wall orientations were expressed as $x = 0$ and $y = 0$. According to Aizu[32] and Sapriel[33], the equations of the twin domain walls reflected the ferroelasticity of the *4/mmmFmmm*. Hence, our results are thought to support the mechanism of ferroelastic twin domains. As a result, the separation of two ^{14}N NMR lines into four ^{14}N NMR lines under T_{C2} was due to the ferroelastic twin domain structure.

Conclusion

To investigate the physical properties of $[(CH_2)_3(NH_3)_2]CuCl_4$ perovskite crystals, we performed DSC, TGA, optical polarizing microscopy, and NMR spectroscopy. The structural roles of the $[(CH_2)_3(NH_3)_2]^+$ cation in $[(CH_2)_3(NH_3)_2]CuCl_4$ crystals were investigated by ^1H MAS NMR, ^{13}C CP/MAS NMR, and ^{14}N static NMR as a function of temperature. The changes in chemical shifts in the ^1H and ^{13}C NMR spectra indicated changes in crystallographic symmetry. The NMR chemical shifts were related to the local field at the location of the resonating nucleus in the crystals. The ^1H NMR chemical shift for NH_3 changed more significantly with temperature than that of CH_2 because being H-bonded, the ^1H NMR chemical shift of the NH_3 moiety is much more sensitive to temperature fluctuations, and varies significantly due to the variation in H-bond length with temperature. The ^{13}C NMR chemical shift for CH_2-1 increased slowly with increasing temperature, without any anomalous change. However, the shift for CH_2-2, moved significantly to lower values with increasing temperature compared to CH_2-1. The ^{13}C NMR chemical shifts of CH_2-2 closer to the N–H···Cl bonds were higher those of CH_2-1. In addition, the abrupt change in the resonance frequency of the ^{14}N nuclei observed near T_{C2} was attributed to a ferroelastic phase transition. The previously reported phase transition at T_{C2}[20] was not observed in DSC, but the ^{14}N NMR data clearly indicated changes in atomic configuration at this temperature. The NH_3 groups are coordinated by N–H···Cl bonds; thus, atomic displacements with temperature in the environment of the ^{14}N nuclei are correlated with $CuCl_4$.

^1H and ^{13}C $T_{1\rho}$ have lower values in the order of milliseconds because $T_{1\rho}$ is inversely proportional to the square of the magnetic moment of paramagnetic ions. The $T_{1\rho}$ values for CH_2 and NH_3 protons were almost independent of temperature, but the CH_2 moiety located in the middle of the N–C–C–C–N bond undergoes tumbling motion according to the BPP theory. The increase in ^{13}C $T_{1\rho}$ at high temperatures may be simply due to the change in distance rather than the change in correlation time. More importantly, the total correlation time τ_C is dominated by the electric relaxation correlation time, rather than the rotational correlation time of the paramagnetic.

Received: 21 September 2020; Accepted: 16 November 2020
Published online: 30 November 2020

References

1. Iqbal, Z., Arend, H. & Wachter, P. Raman scattering from layer-type magnets: $(CH_2)_n(NH_3)_2CuCl_4$, n=2,3 and 5. *J. Phys C: Solid State Phys.* **13**, 4757 (1980).
2. Snively, L. O., Tuthill, G. F. & Drumheller, J. E. Measurement and calculation of the superexchange interaction through the two-halide bridge in the eclipsed layered compounds $(NH_3(CH_2)_nNH_3]CuX$ for n=2-5 and X=$C1_4$ and Cl_2Br_2. *Phys. Rev. B* **24**, 5349 (1981).
3. Mostafa, M. F. & Youssef, A. A. A. Magnetic and electric studies of a new Cu(II) perovskite-like materal. *Z. Naturforsch A* **59**, 35 (2004).
4. Mostafa, M. F. & El-Khiyami, S. S. Crystal structure and electric properties of the organic-inorganic hybrid: $[(CH_2)_6(NH_3)_2]ZnCl_4$. *J. Solid State Chem.* **209**, 82 (2014).
5. Staskieqicz, B., Turowska-Tyrk, I., Baran, J., Gorecki, C. Z. & Czapla, Z. Structural characterization, thermal, vibrational properties and molecular motions in perovskite-type diamonopropanetetrachlorocadmate $NH_3(CH_2)_3NH_3CdCl_4$ crystal. *J. Phys. Chem. Solids* **75**, 1305 (2014).
6. Staskiewicz, B., Czupinski, O. & Czapla, Z. On some spectroscopic properties of a layered 1,3-diammoniumpropylene tetrabromocadmate hybrid crystal. *J. Mol. Struct.* **1074**, 723 (2014).
7. Abdel-Adal, S. K. & Abdel-Rahman, A. S. Synthesis, structure, lattice energy and enthalpy of 2D hybrid perovskite $[NH_3(CH_2)_4NH_3]CoCl_4$, compared to $[NH_3(CH_2)_nNH_3]CoCl_4$, n=3-9. *J. Cryst. Growth.* **457**, 282 (2017).
8. Abdel-Adal, S. K., Kocher-Oberlehner, G., Ionov, A. & Mozhchil, R. N. Effect of organic chain length on structure, electronic composition, lattice potential energy, and optical properties of 2D hybrid perovskites $[(NH_3)(CH_2)_n(NH_3)]CuCl_4$, n = 2–9. *Appl. Phys. A* **123**, 531 (2017).
9. Elseman, A. M. *et al.* Copper-substituted lead perovskite materials constructed with different halides for working $(CH_3NH_3)_2CuX_4$-based perovskite solar cells from experimental and theoretical view. *ACS Appl. Mater. Interfaces* **10**, 11699 (2018).
10. Aramburu, J. A., Garcia-Fernandez, P., Mathiesen, N. R., Garcia-Lastra, J. M. & Moreno, M. Changing the usual interpretation of the structure and ground state of Cu^{2+}-layered perovskites. *J. Phys. Chem. C* **122**, 5071 (2018).
11. Rao, C.N.R., Cheetham, A.K., Thirumurugan, A. Hybrid inorganic-organic materials: A new family in condensed matter physics. *J. Phys.: Condens. Matter* **20**, 83202 (2008).
12. Yadav, R. *et al.* Dielectric and Raman investigations of structural phase transitions in $(C_2H_5NH_3)_2CdCl_4$. *Phys. Chem. Chem. Phys.* **17**, 12207 (2015).
13. Zolfaghari, P.; de Wijs, G.A.; de Groot, R.A. The electronic structure of organic-inorganic hybrid compounds: $(NH_4)_2CuCl_4$, $(CH_3NH_3)_2CuCl_4$ and $(C_2H_5NH_3)_2CuCl_4$. *J. Phys.: Condens. Matter* **25**, 295502 (2013).
14. Arkenbout, A. H., Uemura, T., Takeya, J. & Palstra, T. T. M. Charge-transfer induced surface conductivity for a copper based inorganic-organic hybrid. *Appl. Phys. Lett.* **95**, 173104 (2009).
15. Lim, A. R. Ionic dynamics of the cation in organic-inorganic hybrid compound $(CH_3NH_3)_2MCl_4$ (M=Cu and Zn) by ^1H MAS NMR, ^{13}C CP MASNMR, and ^{14}N NMR. *RSC Adv.* **8**, 18656 (2018).
16. Salje, E. K. H. *Phase Transitions in Ferroelastic and Co-Elastic Crystals* (Cambridge University Press, Cambridge, 1990).
17. Hermes, I. M. *et al.* Ferroelastic fingerprints in methylammonium lead iodide perovskite. *J. Phys. Chem.* **120**, 5724 (2016).
18. Strelcov, E. *et al.* $CH_3NH_3PbI_3$ perovskites: Ferroelasticity revealed. *Sci. Adv.* **3**, e1602165 (2017).
19. Liu, Y. *et al.* Chemical nature of ferroelastic twin domains in CH3NH3PbI3 perovskite. *Nat. Mater.* **17**, 1013 (2018).
20. Mostafa, M. F., Youssef, A. A. A., Montasser, S. S. & Khyami, S. S. The frequency dependence of the conductivity and dielectric relaxation of $[(CH_2)_3(NH_3)_2]Cu(II)Cl_4$. *Z. Naturforsch A* **60**, 837 (2005).
21. Phelps, D.W., Losee, D.B., Hatfield, W.E., Hodgson, D.J. Two-dimensional magnetic systems. Structural and magnetic characterization of bis(propylene-1, 3,-diammonium) tetrachlocuprate(II). *Inorgan. Chem.* **15**, 3147 (1976).
22. Czapla, Z. *et al.* Structural phase trasition in a perovskite-type $NH_3(CH_2)_3NH_3CuCl_4$ crystal X-ray and optical studies. *Phase Transit.* **90**, 637 (2017).
23. Czupinski, O., Ingram, A., Kostrzewa, M., Przeslawski, J. & Czapla, Z. On the structural phase transition in a perovskite-type diaminopropanetrachlorocuprate (II) $NH_3(CH_2)_3NH_3CuCl_4$ crystal. *Acta Phys. Polon. A* **31**, 304 (2017).

24. Guan, X. & Stark, R. E. A general protocol for temperature calibration of MAS NMR probes at arbitrary spinning speeds. *Solid State Nucl. Mag. Reson.* **38**, 74 (2010).
25. Abragam, A. *The Principles of Nuclear Magnetism* (Oxford University Press, Oxford, 1961).
26. Koenig, J. L. *Spectroscopy of Polymers* (Elsevier, New York, 1999).
27. Harris, R. K. *Nuclear Magnetic Resonance Spectroscopy* (Pitman, London, 1983).
28. Morcombe, C. R. & Zilm, K. W. Chemical shift referencing in MAS solid state NMR. *J. Mag. Reson.* **162**, 479 (2003).
29. Bloembergen, N., Purcell, E. M. & Pound, R. V. Relaxation effects in nuclear magnetic resonance absorption. *Phys. Rev.* **73**, 679 (1948).
30. Seliger, J., Blinc, R., Arend, H. & Kind, R. Proton-^{14}N double resonance study of the structural phase transitions in the perovskite type layer compound $(CH_3NH_3)_2CdCl_4$. *Z. Phys. B* **25**, 189 (1976).
31. Mulla-Osman, S., Michel, D., Czapla, Z. ^{14}N NMR study of the domain structure of tetramethylammonium cadmium chloride (TMCC). *Phys. Stat. Sol.* (b) **236**, 173 (2003).
32. Aizu, K. Determination of the state parameters and formulation of spontaneous strain for ferroelastics. *J. Phys. Soc. Japan.* **28**, 706 (1970).
33. Sapriel, J. Domain-wall orientations in ferroelastics. *Phys. Rev. B* **12**, 5128 (1975).

Acknowledgments

This research was supported by the Basic Science Research program through the National Research Foundation of Korea (NRF), funded by the Ministry of Education, Science, and Technology (2018R1D1A1B07041593 and 2016R1A6A1A03012069).

Author contributions

A.R.L. designed the project, performed NMR experiments, and wrote the manuscript.

Competing interests

The author declares no competing interests.

Additional information

Supplementary information is available for this paper at https://doi.org/10.1038/s41598-020-77931-0.

Correspondence and requests for materials should be addressed to A.R.L.

Reprints and permissions information is available at www.nature.com/reprints.

Publisher's note Springer Nature remains neutral with regard to jurisdictional claims in published maps and institutional affiliations.

Open Access This article is licensed under a Creative Commons Attribution 4.0 International License, which permits use, sharing, adaptation, distribution and reproduction in any medium or format, as long as you give appropriate credit to the original author(s) and the source, provide a link to the Creative Commons licence, and indicate if changes were made. The images or other third party material in this article are included in the article's Creative Commons licence, unless indicated otherwise in a credit line to the material. If material is not included in the article's Creative Commons licence and your intended use is not permitted by statutory regulation or exceeds the permitted use, you will need to obtain permission directly from the copyright holder. To view a copy of this licence, visit http://creativecommons.org/licenses/by/4.0/.

© The Author(s) 2020